MODELING OF SUPERSONIC TURBULENT FLOWS IN THE VICINITY

OF AXISYMMETRIC CONFIGURATIONS

I. A. Bedarev, A. V. Borisov, and N. N. Fedorova

UDC 532.517.4 : 533.601.155

Calculation results of turbulent flows in the vicinity of axisymmetric configurations of the cylinder-flare type for Mach numbers M = 3, 5, and 7 are presented. The calculations are performed for conditions of real physical experiments. The mathematical model is based on the averaged Navier–Stokes equations supplemented by the Wilcox turbulence model. The calculated and experimental distributions of pressure on the body surface, velocity fields, and heat-transfer coefficients are compared.

Introduction. The possibilities of predicting the properties of axisymmetric flows in the vicinity of a cylinder-flare configuration for Mach numbers M = 3, 5, and 7 by means of the turbulence model and computational method previously used to calculate plane supersonic flows [1, 2] and a cone–flare configuration are analyzed [3]. The calculations of the cylinder-flare configuration are performed for conditions of real physical experiments suggested as AGARD test cases. Knight and Degrez [4] reported that only one variant of turbulent flow was calculated. The calculated results presented in [4] for distributions of pressure and Stanton number along the model surface for M = 5 are not in very good agreement with experimental data, in particular, the separation-region length is underestimated in calculations. In the present work, we consider most of the two-dimensional turbulent test flows and make an attempt to describe them within the framework of a single model of turbulence and computation method.

Flow Pattern and Main Parameters. Figure 1 shows the flow pattern in the vicinity of the cylinder-flare configuration for the case where the shock wave is capable of separating the boundary layer developing on the cylinder surface (α is the flare angle determining, together with the free-stream Mach number, the possibility of flow separation).

The test conditions for which the present calculations were performed are listed in Table 1 (T_0 is the stagnation temperature, Re_1 is the unit Reynolds number, and δ is the boundary-layer thickness on the cylinder surface ahead of the interaction region).

Basic Equations and Numerical Algorithm. The main mathematical model used in the present work is the system of Favre-averaged full Navier–Stokes equations, which describe the motion of a viscous compressible heat-conducting gas. To close the averaged equations, we used the two-parameter k–ω turbulence model proposed by Wilcox [5, 6]. A detailed description of the mathematical model can be found in [3].

The steady solution of the system of differential equations was found by the pseudo-transient method on the basis of an implicit four-step finite-difference system of the unified-algorithm type [7] with the use of splitting with respect to physical processes and spatial variables. The Navier–Stokes equations were solved first, and then turbulent quantities were determined for the calculated gas-dynamic parameters from the differential equations of the turbulence model. The TVD approach based on the method of flux-vector splitting with respect to physical processes [7] and the van Leer flux-vector splitting method [8] were used.

The computational domain is bounded by the body surface from below and by the upper, input, and output sections from above, on the left, and on the right, respectively, which are located rather far from the interaction
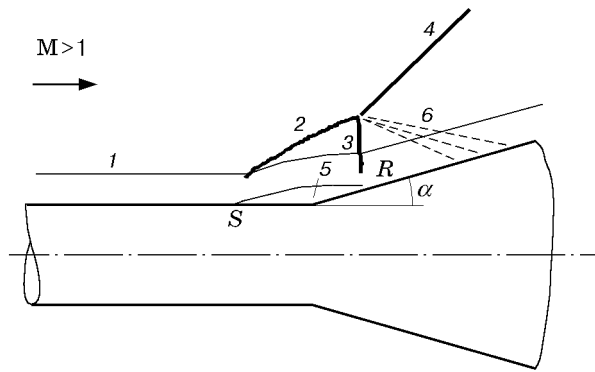
Fig. 1. Flow pattern: 1) boundary-layer edge; 2) separation shock; 3) reattachment shock; 4) main shock wave; 5) separation region; 6) expansion fan emanating from the triple point of the λ-configuration; the points of flow separation and reattachment are indicated by the letters S and R.

TABLE 1

Variant No.	M	Re_1, 1/m	α, deg	T_0, K	δ, mm	Flow regime
1	2.85	$1.60 \cdot 10^7$	30	265	11.0	Separated
2	5.00	$4.41 \cdot 10^7$	35	500	2.5	Separated
3	7.05	$5.66 \cdot 10^6$	20	890	2.5	Attached
4	7.05	$5.66 \cdot 10^6$	30	890	2.5	Separated
5	7.05	$5.66 \cdot 10^6$	35	890	2.5	Separated

region. No-slip conditions were imposed for velocity on the cylinder surface, and the absence of heat fluxes or a constant temperature were set depending on conditions of a particular problem. Nonreflecting "simple" wave conditions were imposed at the upper boundary, which ensured free outflow from the computational domain. Since all cases considered were supersonic, the so-called soft conditions for all calculation parameters were used in the output cross section. The free-stream parameters were set in the external region of the input cross section, and profiles of all calculation parameters obtained by solving simplified equations for the turbulent boundary layer and matching available experimental data in terms of the skin-friction coefficient and integral values were prescribed in the near-wall region.

A regular computational grid condensing toward the surface was used. In most calculations, the grid contained 250 nodes in the streamwise direction and 100 nodes in the normal-to-wall direction. To study grid convergence, some variants were calculated using grids with 125×100, 500×100, and 250×200 nodes. For each calculated case, the mandatory condition was that several grid nodes in the radial direction were located in the laminar sublayer.

A detailed description of the numerical algorithm can be found in [9]. This method yielded good results in numerical simulation of supersonic turbulent separated flows in the vicinity of plane configurations [1, 2].

Calculation Results. The calculation results were compared with experimental data in terms of all flow parameters available in the experimental database: pressure and heat-transfer distributions and pressure and velocity profiles.

The experimental and calculated pressure distributions for variant No. 1 (see Table 1) are compared in Fig. 2 (P_{w1} is the pressure ahead of the interaction region). The calculations were performed with the use of the method of splitting with regard to physical processes [7] and van Leer method [8]. It follows from Fig. 2 that both methods correctly predict the distance where the pressure increase begins but underestimate the pressure behind the interaction region. The reason may be a more downstream position of the reattachment point in calculations as compared to the experiment.

Figure 3 shows the calculated and experimental mean-velocity profiles for variant No. 1. It follows from Fig. 3 that reattachment in calculations occurs more downstream than in the experiment. It should be noted that the calculation results obtained by the method of [7] are in better agreement with experimental data in regions of flow separation and reattachment.
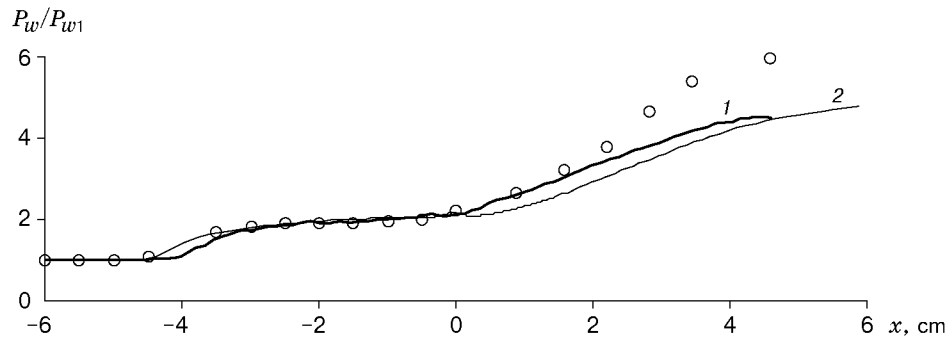
Fig. 2. Experimental (points) and calculated (curves) static pressure distributions over the surface for variant No. 1: curves 1 and 2 refer to calculations by the schemes of [7] and [8], respectively.
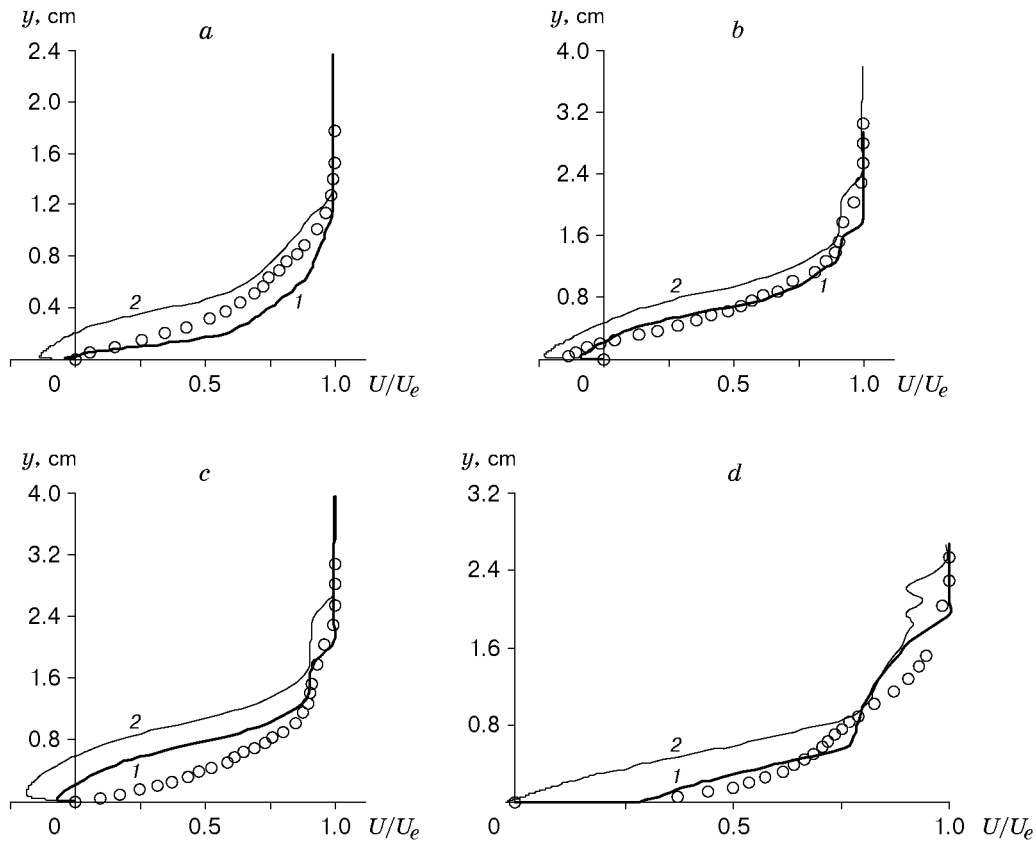

Fig. 3. Experimental (points) and calculated (curves) mean-velocity profiles for variant No. 1 for $x = -2.5$ (a), -0.5 (b), 0.88 (c), and 3.98 cm (d): curves 1 and 2 refer to calculations by the schemes of [7] and [8], respectively.

Figure 4 shows the calculated and experimental distributions of pressure and Stanton numbers on the body surface for variant No. 2. The agreement in terms of the separation-region length and maximum pressures behind the shock waves should be noted. The calculations reproduce the position and intensity of expansion waves emanating from the triple point of the λ-configuration. Nevertheless, these waves produce a stronger decrease in heat fluxes as compared to the experiment (Fig. 4b).

The possibility of separated flow controlling by means of the temperature factor follows from Fig. 5, which shows the distributions of static pressure and skin-friction coefficient on the body surface for variant No. 2. The wall temperature was varied in calculations. The value $T_w = 380$ K is close to the adiabatic temperature. It follows from Fig. 5 that a decrease in temperature reduces the separation region and alters the skin-friction coefficient C_f behind the reattachment point.
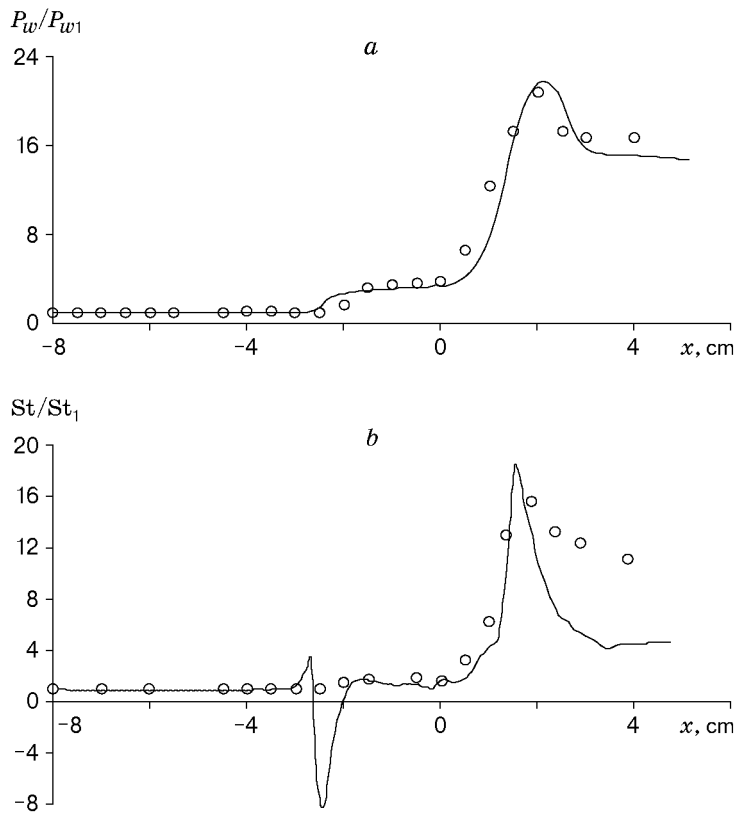
863

Fig. 4. Calculated (curves) and experimental (points) distributions of pressure (a) and Stanton numbers (b) on the model surface for variant No. 2.
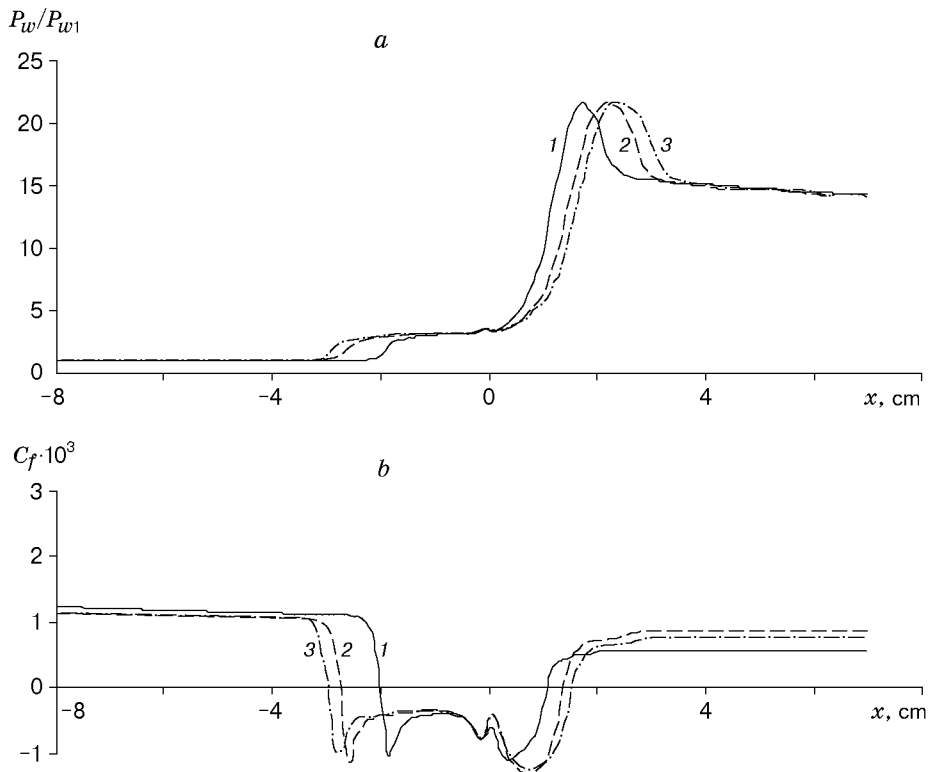

Fig. 5. Distributions of static pressure (a) and skin friction (b) on the body surface for variant No. 2 for $T_w = 300$ (curve 1), 360 (curve 2), and 380 K (curve 3).
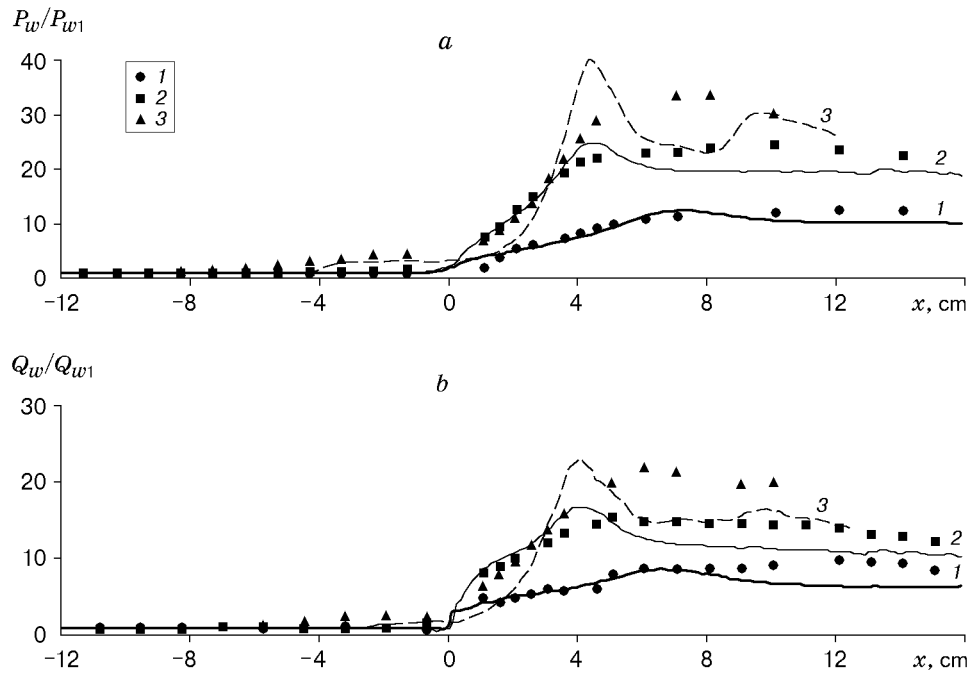
Fig. 6. Calculated (curves) and experimental (points) distributions of pressure (a) and heat-transfer coefficients (b) for variant Nos. 3 (1), 4 (2), and 5 (3).
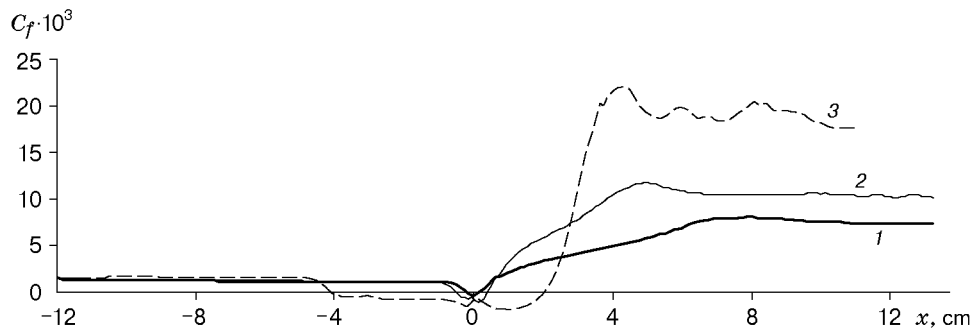

Fig. 7. Calculated dependence $C_f(x)$ for variant Nos. 3 (1), 4 (2), and 5 (3).

Evolution of the separated flow with increasing angle of the flare for M $=$ 7 was also considered. The method of splitting with respect to physical processes was used in calculations. The calculation results for variant Nos. 3–5 (see Table 1) are plotted in Figs. 6 and 7. In variant No. 3 ($\alpha = 20°$), an attached flow was registered in the experiment. The calculated values of the skin-friction coefficient become negative only in the vicinity of the point $x = 0$, and the pressure distribution has no typical plateau formed above the separation region. An increase in the flare angle up to 30° leads to the growth of the separation region (see Fig. 7). In variant No. 5 ($\alpha = 35°$), a considerable separation region appears in the region $x = (-3)$–1 cm. A typical plateau is observed in the pressure distribution because of the presence of the separation region. For variant Nos. 3–5, the calculation results in the region behind the shock wave are in good agreement with experimental data. Behind the interaction region, however, there is some difference (approximately 10%). In this calculation variant, as in variant No. 2, expansion waves incident onto the surface from the triple point of the λ-configuration are obtained in the region $x = 4$–8 cm. Such intense expansion waves were not observed in the experiment. In this case, flow reattachment in calculations occurs later than in the experiments. The drawback of the numerical solution for variant No. 5 is also a more intense increase in pressure and heat-transfer intensity in the reattachment region. The reason for this disagreement may be the underestimated values of turbulent viscosity in the interaction region in calculations or the neglect of nonequilibrium chemical processes in hypersonic flows.

Conclusions. The calculations of supersonic and hypersonic flows around a cylinder-flare configuration show that the chosen computational algorithm and turbulence model allow obtaining good agreement of calculated and experimental data for axisymmetric flows with various Mach numbers. Rather good agreement of calculated and experimental results is observed in using the Wilcox turbulence model without corrections for the compressibility effect up to $M = 7$. The temperature factor is shown to exert a significant effect on evolution of the separated flow.

The difference in calculated and experimental data in some regions can be attributed to the imperfect computational method and turbulence model. By an example of variant No. 1, it is shown that two methods for inviscid-flow approximation used yield different positions of flow separation and reattachment points. The lower (as compared to the experiment) heat-transfer intensity in expansion waves in variant No. 2 can be explained by a greater decrease in the level of turbulent fluctuations in expansion waves emanating from the triple point of the λ-configuration. A similar effect was observed in calculating flows near steps [2]. In addition, the differences may be caused by the absence of information on boundary-layer parameters upstream of interaction, such as the integral boundary-layer thicknesses and skin-friction coefficient, which exert a significant effect on the formation of the separation region of the turbulent boundary layer and are necessary for defining the profiles of turbulent parameters in the input cross section of the computational domain. Since these data are absent for some cases in the database used, arbitrary values were used for these parameter in calculations. The calculations also ignored some physical features essential for flows with boundary-layer separation, in particular, flow unsteadiness, which is difficult to take into account in the pseudo-transient method, and external turbulence level.

REFERENCES

1. A. V. Borisov, A. A. Zheltovodov, A. I. Maksimov, et al., "Experimental and numerical study of supersonic turbulent separated flows near two-dimensional obstacles," *Izv. Ross. Akad. Nauk, Mekh. Zhidk. Gaza*, No. 2, 26–37 (1999).
2. I. A. Bedarev and N. N. Fedorova, "Computation of gas-dynamic parameters and heat transfer in supersonic turbulent separated flows near backward-facing steps," *J. Appl. Mech. Tech. Phys.*, **42**, No. 1, 49–56 (2001).
3. I. A. Bedarev, A. A. Maslov, A. A. Sidorenko, et al., "Experimental and numerical study of a hypersonic separated flow in the vicinity of a cone–flare model," *J. Appl. Mech. Tech. Phys.*, **43**, No. 6, 867–876 (2002).
4. D. D. Knight and G. Degrez, "Shock wave boundary layer interactions in high Mach number flows. A critical survey of current CFD prediction capabilities," AGARD Advisory Report No. 319, Part 2 (1998), pp. 1.1–1.35.
5. D. C. Wilcox, *Turbulence Modeling for CFD*," DCW Industr. Inc., California, La Caňada (1993).
6. D. D. Knight, "Numerical simulation of compressible turbulent flows using the Reynolds-averaged Navier–Stokes equations," in: *Turbulence in Compressible Flows*, AGARD Rep. No. 819 (1997), pp. 5-1–5-52.
7. V. M. Kovenya and N. N. Yanenko, *Method of Splitting in Gas-Dynamic Problems* [in Russian], Nauka, Novosibirsk (1981).
8. B. Van Leer, "Flux-vector splitting for the Euler equations," *Lecture Notes Phys.*, **170**, 507–512 (1982).
9. A. V. Borisov and N. N. Fedorova, "Numerical simulation of turbulent flows near forward-facing steps," *Thermophys. Aeromech.*, **4**, No. 1, 69–83 (1996).